Specific absorbed fractions of electrons and photons for Rad-HUMAN phantom using Monte Carlo method *

WANG Wen(王文)[1,2] CHENG Meng-Yun(程梦云)[2] LONG Peng-Cheng(龙鹏程)[2] HU Li-Qin(胡丽琴)[1,2;1)]

[1] University of Science and Technology of China, Hefei 230027, China
[2] Key Laboratory of Neutronics and Radiation Safety, Institute of Nuclear Energy Safety Technology, Chinese Academy of Sciences, Hefei 230031, China

Abstract: The specific absorbed fractions (SAF) for self- and cross-irradiation are effective tools for the internal dose estimation of inhalation and ingestion intakes of radionuclides. A set of SAFs of photons and electrons were calculated using the Rad-HUMAN phantom, which is a computational voxel phantom of a Chinese adult female that was created using the color photographic image of the Chinese Visible Human (CVH) data set by the FDS Team. The model can represent most Chinese adult female anatomical characteristics and can be taken as an individual phantom to investigate the difference of internal dose with Caucasians. In this study, the emission of mono-energetic photons and electrons of 10 keV to 4 MeV energy were calculated using the Monte Carlo particle transport calculation code MCNP. Results were compared with the values from ICRP reference and ORNL models. The results showed that SAF from the Rad-HUMAN have similar trends but are larger than those from the other two models. The differences were due to the racial and anatomical differences in organ mass and inter-organ distance. The SAFs based on the Rad-HUMAN phantom provide an accurate and reliable data for internal radiation dose calculations for Chinese females.

Key words: dose assessment, SAF, AF, *S* values, phantom, Rad-HUMAN

PACS: 87.57.uq, 87.53.Jw, 87.10.Rt **DOI:** 10.1088/1674-1137/39/7/078203

1 Introduction

Absorbed fractions (AFs) and specific absorbed fractions (SAFs) that account for the partial deposition of radiation energy in target organs and tissues are essential for the calculation of radiation dose of the intakes of radionuclides or a nuclear medicine procedure. The Medical Internal Radiation Dosimetry (MIRD) Committee provides a systematic approach of internal dose calculation which is known as the MIRD schema [1, 2]. To obtain the SAFs, AFs and other conversion coefficients, computational phantoms and Monte Carlo methods are often used. Photon SAFs were calculated using MIRD-type mathematical anthropomorphic phantoms of different ages. The mathematical models were first designed by Fisher and Snyder from the Oak Ridge National Laboratory (ORNL) in 1969 [3] and were revised in 1978 [4]. They were adopted by the Medical Internal Radiation Dose (MIRD) Committee as MIRD-type models, and have been evolved into several improved and extended versions for dosimetry calculation [5–7]. The MIRD models facilitate rapid dose calculation but suffer from the loss of most anatomical details.

To perform accurate absorbed-dose calculation, voxel models were developed based on computed tomography (CT), magnetic resonance imaging (MRI) or colored photographs which can provide more realistic and detailed information of the human anatomy. Second generation phantoms, using medical image data of real human bodies, is now used for internal dosimetry and can significantly contribute to better dose assessment. Nowadays, many individual voxel-based models have been reported [8–11]. Many studies reveal that, due to the simplified inequalities used to described the organs in MRID models, the inter-organ distances, organ shape and location are different from reality. For internal dosimetry, the influencing parameters are the relative position of the source and target organs and organ mass. This leads to higher values of SAFs for many source - target organ combinations for the voxel models, especially for lower photon energy [12]. Consequently, voxel phantoms could significantly contribute to improved dose assessment for patients. So, the International Commission on Radiological Protection (ICRP) and the International Commiss-

Received 2 November 2014

∗ Supported by Strategic Priority Research Program of Chinese Academy of Sciences (XDA03040000), National Natural Science Foundation of China (910266004, 11305205, 11305203) and National Special Program for ITER (2014GB112001)

1) E-mail: liqin.hu@fds.org.cn

ion of Radiation Units and Measurements (ICRU) decided to use voxel-based models as a reference model to improve reference dosimetry [13] and the reference dosimetric parameters including SAFs are calculated using the new ICRP/ICRU adult reference phantoms [14].

Much tabulation of SAFs has been derived from Monte Carlo transport simulations using stylized computational models or voxel models to represent human internal organ anatomy. However, most of the phantoms are based on medical images of Caucasian people and may not be completely appropriate for application in China. Internal radiation dose calculations built on a Chinese voxel model are becoming more and more important for nuclear medicine. Qiu et al. established the Chinese mathematical phantom to calculate the photon SAFs and compared with ORNL phantoms [15]. Liu Yang et al. calculated the photon and electron SAFs based on the VCH voxel model by color photographs of an adult male cadaver [16]. However, there is very limited work on the use of voxel models to represent the Chinese female calculated SAFs for internal dosimetry.

A voxel model of a Chinese adult female named Rad-HUMAN [17] was created using the color photographic images of the Chinese Visible Human (CVH) data set by the FDS Team. A set of SAFs for monoenergetic photon and electrons were calculated using Rad-HUMAN, which can represent the Chinese female. This paper analyses the first set of SAFs calculated with the Chinese female phantom by comparing the results with those of the ICRP Ref. [14] and ORNL models. Dosimetric differences between mathematical and voxel models and those between the Chinese and Caucasian models will also be discussed in this paper.

2 Materials and methods

2.1 Rad-HUMAN phantom

The high-resolution color photographic images of the CVH data set were obtained from a 22-year-old Chinese female cadaver. The candidate was 162 cm in height and 54 kg in weight, which is close to the Chinese reference adult female [17]. The Rad-HUMAN which is shown in Fig. 1 was constructed through three steps: 1) identify and segment the organs and tissues in the color photographic images to yield 46 organs and tissues by experienced anatomists; 2) assign the organs and tissues with density and chemical composition that is recommended in ICRP 89 [18] and the International Commission on Radiation Units and Measurements (ICRU) 44 Report [19]; 3) describe the anatomical data into a Monte Carlo code input file [20]. After that, a voxel-based phantom that represented the average anatomical characteristics of the Chinese female population was established for radiation dosimetry.

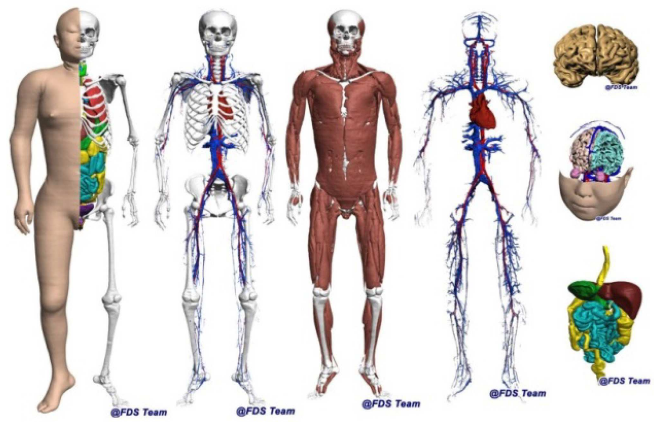

Fig. 1. (color online) 3D view of Rad-HUMAN.

However, manual description and verification of computational phantoms for MC simulation are tedious, error-prone and time-consuming. SuperMC/MCAM is a Multi-Physics Coupling Analysis Modeling Program [21–24] developed by the FDS Team [25–30]. Automatic conversion from CT/segmented sectioned images to a human computational phantom can be performed by SuperMC/MCAM.

A whole-body computational phantom of a Chinese female called Rad-HUMAN was created by SuperMC/MCAM using colored photographic images. Rad-HUMAN contains 46 organs and tissues and is divided into more than 28.8 billion voxels, with 0.15 mm×0.15 mm×0.25 mm voxel division for head and neck regions and 0.15 mm×0.15 mm×0.5 mm for other regions.

2.2 Monte Carlo calculations

The Monte Carlo method has been widely used in situations where physical measurements and analytical calculations are either inconvenient or impossible. MCNP is a general-purpose Monte Carlo code designed to transport neutrons, photons and electrons in an arbitrarily assigned three-dimensional geometry. In this study, the Rad-HUMAN phantom was implemented in the Monte Carlo particle transport code MCNP by repeated structure to describe the model. The density and element/chemical composition of organs and tissues acquired from ICRP 89 and ICRU Report 44 were used in the Monte Carlo simulations. According to the ORNL SAF data, mono-energetic and isotropic photon and electron sources were selected with discrete energy ranging from 10 keV to 4 MeV. Ten million electrons and photons were tracked per source region and energy in MCNP calculations.

MCNP offers a variety of variance reduction techniques based on different nonanalog simulations. It is important to use these techniques for the difficult problems to obtain both precise and computationally efficient results for solving difficult problems. It is difficult to obtain accurate SAFs when the target organ is small. There are three widely used variance reduction techniques to solve this problem: geometry splitting and Russian roulette, DXTRAN spheres and forced collisions (FCL).The forced collisions (FCL) method, which is more efficient than the other two methods, was used in this simulation. The cutoff energies for both photons and electrons were set with the default values of 1 keV.

2.3 Calculation method of SAFs

The SAF is an important quantity of organ self-dose and cross-dose for an internal irradiation scenario. AF specify the fraction of energy emitted by radioactivity in source organ (r_S) that is absorbed in the source organ itself and in target organs (r_T). SAF is AF divided by target organ mass. According to the MIRD formalism [31], the equations related to absorbed dose, S values and the SAFs are as follows:

$$D(r_\mathrm{T},T_\mathrm{D})=\sum_{r_\mathrm{S}}A(r_\mathrm{S},T_\mathrm{D})\cdot S(r_\mathrm{T}\leftarrow r_\mathrm{S}), \tag{1}$$

where $D(r_\mathrm{T}, T_\mathrm{D})$ is the absorbed dose in the target. $\mathrm{A}(r_\mathrm{T}, T_\mathrm{D})$ is the time-integrated or cumulated activity in the source organ. $S(r_\mathrm{T}\leftarrow r_\mathrm{S})$ is the so-called S value in $\mathrm{Gy}\cdot\mathrm{MBq}^{-1}\cdot\mathrm{S}^{-1}$ defined as the mean absorbed dose rate to the target organ per nuclear transition in the source tissue.

$$S(r_\mathrm{T}\leftarrow r_\mathrm{S})=\sum_{\mathrm{i}}E_\mathrm{i}Y_\mathrm{i}(r_\mathrm{s},T_\mathrm{D})\cdot SAF(r_\mathrm{T}\leftarrow r_\mathrm{S},E_\mathrm{i}), \tag{2}$$

where E_i is the mean energy of radiation type i. Y_i is the yield of radiation type i per transformation.

$$SAF(r_\mathrm{T}\leftarrow r_\mathrm{S})=\frac{1}{m_\mathrm{T}}\cdot\varphi_{\mathrm{i}(r_\mathrm{T}\leftarrow r_\mathrm{S})}=\frac{1}{m_\mathrm{T}}\cdot\frac{E_\mathrm{T}}{E_\mathrm{S}}, \tag{3}$$

where m_T is the mass of the target. $\varphi_{\mathrm{i}(r_\mathrm{T}\leftarrow r_\mathrm{S})}$ is the absorbed fraction (AF). E_T is the energy emitted from source organ and E_S is the energy absorbed in target organs [12].

The electron SAFs calculated with Monte Carlo techniques for the Rad-HUMAN phantom were compared with the former assumption of ICRP and MIRD [4, 32] that electrons are fully absorbed in the source organ itself.

3 Results and discussion

The photon and electron SAFs were calculated using the Rad-HUMAN phantom and compared to SAFs calculated using ORNL and ICRP/ICRU reference computational phantom. The SAFs for electrons were calculated using Rad-HUMAN and compared with SAFs from the assumptions of ICRP Publication [32].

3.1 Photon specific absorbed fractions

Figure 2 shows the photon SAFs for self-irradiation. The source organ is also the target organ for the photon energy ranges from 10 keV to 4 MeV in many organs. The photon SAFs for self-irradiation decreases with increasing photon energy from 10–100 keV. At the photon energy of 0.1 MeV, the values begin to increase slightly to a maximum valule of 0.5 MeV and then begin to decrease again. Fig. 2 showed the influence of organ mass on the photon SAFs for self-irradiation. It can be concluded that organs with small mass obtain larger SAFs than big mass organs; organs with the similar masses like kidney and stomach have very small differences in SFAs for self-irradiation.

Specific absorbed fractions (SAFs) for photon cross-absorption with the liver as the source were displayed in Fig. 3. The figure showed that the SAFs of the adrenal

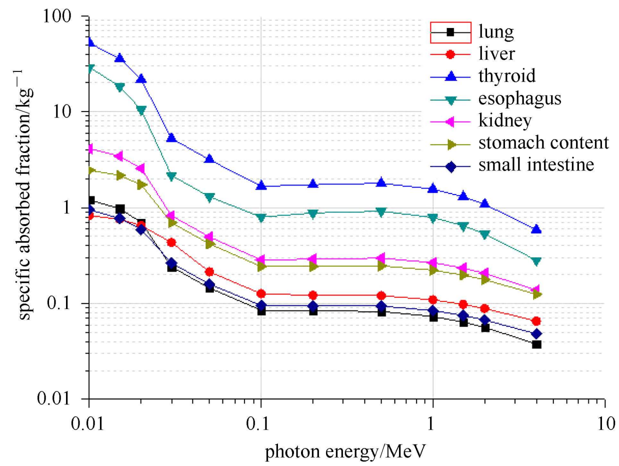

Fig. 2. (color online) SAFs for photon self-absorption in some organs of Rad-HUMAN.

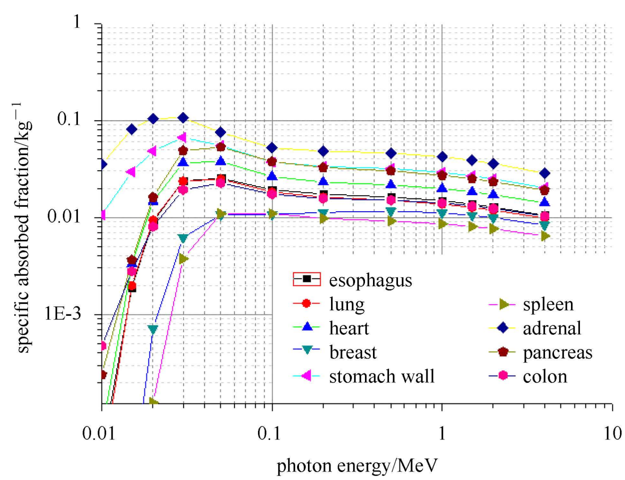

Fig. 3. (color online) SAFs for photon cross-absorption as the source in liver.

gland, which has a small mass, have the larger value, but the SAFs of the esophagus and lung have the large mass and small differences in SAFs. Results show that the organ geometry, density and the distance between source and target have a significant effect on the SAFs for cross-irradiation.

The SAFs using the Rad-HUMAN phantom were compared with SAFs from ORNL and ICRP adult reference phantoms. Fig. 4 shows the SAFs for the photon self-absorption in lungs of the two voxel phantoms and the mathematical phantom. The SAFs for organs in the Rad-HUMAN phantom have a similar tendency to those in the ICRP/ICRU reference phantom and ORNL phantom. The SAFs values for photon self-absorption in the lung were larger than the other models as it has less mass. Variations in SAFs were calculated as the ratio of the Rad-HUMAN to the ORNL and ICRP adult reference phantoms. The average ratio was 20% with the ICRP adult reference phantoms and 48% with the ONRL phantom. In case of self-irradiation, the variations are dependent on the difference in organ mass; the organ geometry does not have a significant influence on the SAF estimation. Fig. 5 shows that the SAFs (lung→stomach wall) using the Rad-HUMAN diverge from the other models. For energy below 0.5 MeV, the ratio reached up to 50% and for higher energy the ratio decreased to 20%. The observed discrepancies are due to different shapes and inter-organ distances between the organs of the phantoms whose influence is quite dominant at low energy.

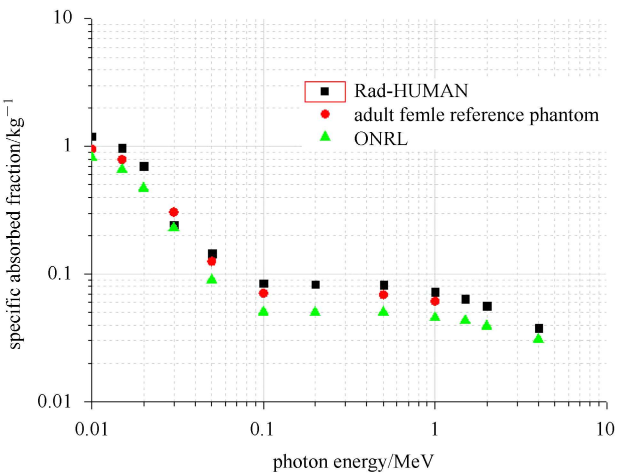

Fig. 4. (color online) SAFs for photon self-absorption in the lung.

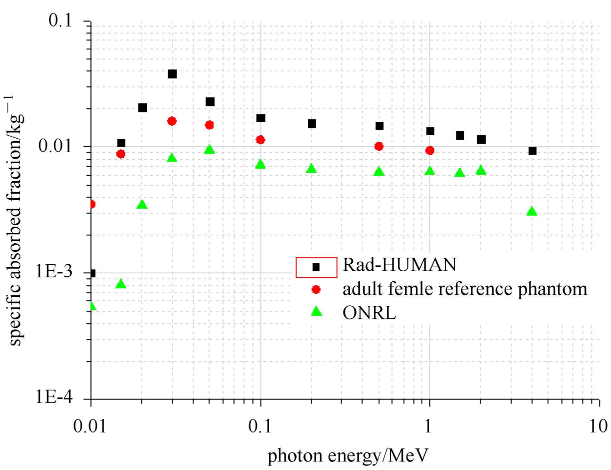

Fig. 5. (color online) SAFs for cross-absorption (lung→stomach wall).

3.2 Electron specific absorbed fractions

Because of the low penetration power of electrons and the previously applied assumption of ICRP Publication 30 [32], which supposed the electrons are fully absorbed in the source organ and electron, AFs are recommended to be 1, AFs and SAFS are recommended to be 0 when the source and the target are different.

Figure 6 and 7 shows the electron SF and SAF values for self-absorption in many organs of the Rad-HUMAN phantom. The SAF values for electrons are different from the simplified assumptions of ICRP Publication 30. From Fig. 6 we can see that electrons have the ability to leave the source organ with electron energy above 0.5 MeV. The self-absorption SAFs are constant and agree with the inverse organ mass for electron energy. For the large organs such as liver and lung, the drop-off of the AFs and SAFs with increasing electron energy is moderate as electron energy increases, since short electron ranges are still in the large source regions. For small organs like the thyroid, the drop-off of the AFs and SAFs are much more pronounced with the increase of electron energy, since even shorter electron ranges could cross the organ boundary.

Figure 8 shows the cross-absorption electron SAF values for source in the stomach content of the Rad-HUMAN phantom. Fig. 8 shows the electron irradiation

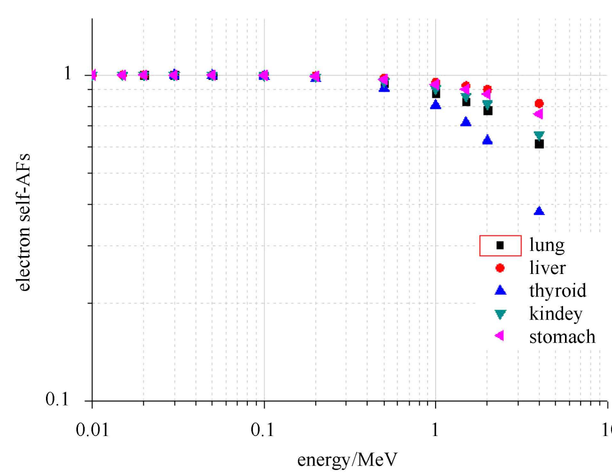

Fig. 6. (color online) AFs for electron self-absorption.

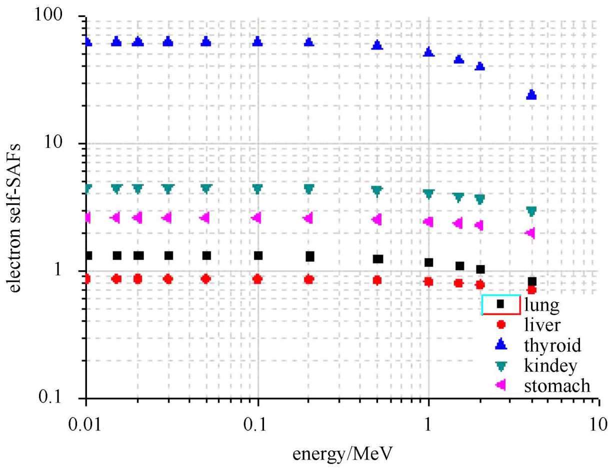

Fig. 7. (color online) SAFs for electron self-absorption.

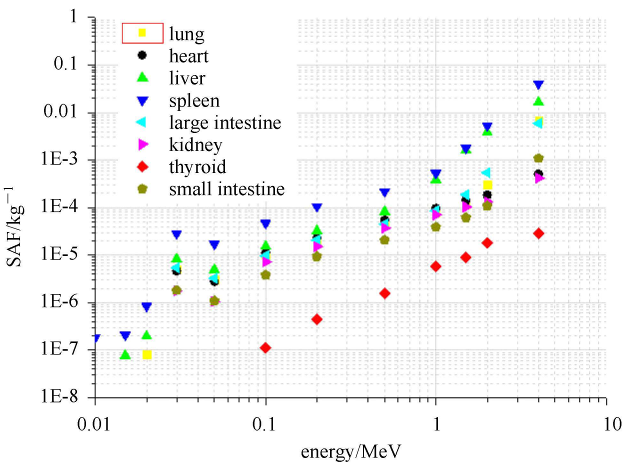

Fig. 8. (color online) Electron SAFs for source in stomach content.

of adjacent regions cannot always be neglected, even though electrons are considered as weak penetrating radiation. Results show that SAF values for distant organs such as the thyroid are smaller than other organs because of short electron ranges. The values for neighboring organs such as the spleen and the liver cannot be negligible for electron energy above 1 MeV.

From the Monte Carlo calculation of electron SAF values, we can conclude that high-energy electrons can cross the source organ boundaries and the ICRP 30 approach assuming full absorption in the source underestimates the absorption of the neighboring organs around the source organs. The SAF value is related to the geometry and distance between the source and organ. The real phantom and Monte Carlo transport method could make the dosimetry calculation clinically possible in nuclear medicine.

3.3 *S* value calculation

Once mono-energetic photon and electron SAFs are assembled, S values for γ- and β-ray emitted from radionuclides were calculated using Eq. (2). In this study, we calculated the radionuclides associated with common molecular studies of ^{99}mTc [33], which are usually used as molecular imaging radionuclides. S values of ^{99}mTc were calculated in the liver and compared with those of VIP-Man, VCH and MIRD as listed in Table 1 [16]. The average dose from a specified radionuclide can be calculated using the S value by Eq. (1). Assuming that 1 mCi ^{99}mTc is distributed uniformly in the liver and there is no biological removal, the mean absorbed doses for a source in the liver to other organs of the Rad-HUMAN were calculated compared with those of VIP-Man, VCH and MIRD as listed in Table 1. The radionuclide ^{99}mTc is a gamma emitter. From the table we can see significant variation in S values and organ doses between those phantoms. The S value of the adrenal gland of the Rad-Human is 62% larger than the S value of the adrenal gland of VCH, 30% larger than the S value of the adrenal gland of VIP-Man and 180% larger than the S value of the adrenal gland of MIRD Pamphlet No. 11. The differences among those phantoms were due to variations in organ mass, organ size and organ contours. Small organs such as the adrenal gland and pancreas are difficult to segment and have irregular shapes. The organs of those

Table 1. Comparisons of S values and mean absorbed doses for organs with 1 mCi ^{99}mTc distributed in liver with VCH, VIP-Man and MRID Pamphlet N0. 11.

organ	Rad-HUMAN S values /(Gy/Bq·s)	dose/mGy	VCH S values /(Gy/Bq·s)	dose/mGy	VIP-man S values /(Gy/Bq·s)	dose/mGy	MIRD pamphlet No.11 S values /(Gy/Bq·s)	dose/mGy
adrenal	9.79E-16	0.96	6.01E-16	0.59	7.48E-16	0.74	3.38E-16	0.33
kidney	3.87E-16	0.38	2.54E-16	0.25	3.65E-16	0.36	2.93E-16	0.29
liver	3.56E-15	3.50	3.49E-15	3.43	3.36E-15	3.30	3.45E-16	3.39
Lung	3.62E-16	0.36	7.77E-16	0.76	2.80E-16	0.28	1.88E-16	0.18
pancreas	3.46E-16	0.34	3.38E-16	0.33	5.50E-16	0.54	3.15E-16	0.31
spleen	2.17E-16	0.21	1.44E-16	0.14	1.27E-16	0.12	6.91E-16	0.07
stomach wall	7.49E-16	0.74	4.59E-16	0.45	4.98E-16	0.49	1.43E-16	0.14
thyroid	4.17E-17	0.04	8.57E-17	0.08	5.06E-17	0.05	1.13E-16	0.01

phantoms may have large differences in size and mass. Differences of S value and organ doses for ^{99}mTc in the liver to other models were primarily due to variations in organ size, volume, mass and inter-organ separation. Based on the Rad-HUMAN phantom and calculation method, we can evaluate the mean absorbed dose of any organs and tissues for radionuclide in source organs of patients.

4 Conclusion

In this study, a new set of SAFs and S values of the Rad-HUMAN were calculated and compared with the SAF data of ORNL and ICRP references phantom. The first set of SAFs using Rad-HUMAN which can represent the Chinese female could make the dosimetry calculation more exact in nuclear medicine for Chinese females. In the present study, it has been confirmed that the SAFs for self-irradiation depend on the energy and the mass of the target/source organ, and the SAFs for cross irradiation depend on the relative position of source to target organs. It can be concluded that SAFs for Rad-HUMAN have the similar trends that validate the data is accurate and reliable for internal radiation dose calculations for Chinese females. The SAFs and S values obtained using the real phantom and connected to individual biokinetic data could make the dosimetry calculation clinically possible in nuclear medicine.

We would like to express our appreciation for the support of the members of the FDS Team. We would like to thank Professor Shaoxiang Zhang et al, from the Third Military Medical University, People' s Republic of China, for providing the visible human anatomical dataset and related support, and Professor X. George Xu for helpful discussion and support during the work.

References

1 Loevinger R, Berman M. MIRD J Nuclear Med., 1968, **9**(Suppl 1): 7–14
2 Loevinger R, Berman M. NM/MIRD Pamphlet no 1, Revised, Society of Nuclear Medicine, NY, 1976
3 Snyder WS, Fisher Jr, Ford MR et al. Nucl. Med., 1969, **3**: 7–52
4 Snyder WS, Ford MR, Warner GG. The Society of Nuclear Medicine, 1978
5 Cristy M. Report ORNL/NUREG/TM-367, Oak Ridge National Laboratory, Oak Ridge, Tenn., USA, 1980
6 Kramer R, Zankl M, Williams G. GSF - Report S-885.Reprint July 1999.Institut für Strahlenschutz, GSF-Forschungszentrum für Umwelt und Gesundheit, Neuherberg-M unchen, 1982
7 Stabin M, Watson E, Cristy M et al. Report No. ORNL/TM-12907, Oak Ridge National Laboratory, Oak Ridge, Tenn., USA, 1995
8 Gibbs SJ, Pujol A Jr, Chen TS et al. Oral. Surg. Oral. Med. O, 1984, **58**: 347–354
9 Zubal I G, Harrell C R, Smith E O et al. Med. Phys., 1994, **21**: 299–302
10 Dimbylow P J. Phys. Med. Biol, 2005, **50**: 1047–1070
11 Xu XG, Chao TC, Bozkurt A. Health Phys., 2000, **78**(5): 476–485
12 Zankl M, Schlattl H, Petoussi-Henss N et al. Voxel Phantoms for internal Dosimetry. Radiation Physics for Nuclear Medicine. Springer Berlin Heidelberg, 2011. 257–279
13 ICRP 2007 Recommendations of the International Commission on Radiological Protection ICRP Publication 103 (Oxford: Elsevier), 2007
14 Hadid L, Desbree A, Schlattl H et al. Phys. Med. Biol. 2010, **55**: 3631–3641
15 QIU R, LI J L, ZHANG Z et al. Health Phys., 2008, **95**: 716–724
16 LIU Yang, XIE Tian-Wu, LIU Qian. Nuclear Science and Techniques, 2011, **22**: 165–173
17 CHENG Meng-Yun. Computational Modeling Method and Its Application. Hefei: Chinese Academy of Science, 2012
18 International Commission on Radiological Protection, Basic Anatomical and Physiological Data for Use in Radiological Protection: Reference Values, ICRP Publication 89, 2003
19 International Commission on Radiation Units and Measurements, Tissue Substitutes in Radiation Dosimetry and Measurement, Bethesda, MD: ICRU; ICRU Report 44, 1989
20 CHENG M Y, ZENG Q, CAO R F et al. Progress in Nuclear Science and Technology (PNST), 2011, **2**: 237–241
21 WU Y, FDS Team. Fusion Engineering and Design, 2009, **84**: 1987–1992
22 WU Y, XIE Z, Fischer U. Nuclear Scinece and Engineering and Design, 2009, **84**(7–11): 1987–1992
23 SONG J, SUN G Y, CHEN Z P et al. Fusion Engineering and Design, 2014, **89**(11): 2499–2503
24 WU Y, SONG J, ZHENG H et al. Annals of Nuclear Energy. DOI:10.1016/j.anucene, 2014, **08**: 058
25 WU Y C, JIANG J Q, WANG M H et al. Nuclear Fusion, 2011, **50**(10): 103036
26 WU Y, CHEN H, LIU S et al. Journal of Nuclear Materials, 2009, **386–388**: 122–126
27 WU Y, FDS Team. Fusion Engineering and Design, 2008, **83**: 1683–1689
28 WU Y, FDS Team. Fusion Engineering and Design, 2006, **81**: 2713–2718
29 WU Y C, QIAN J P, YU J N. Journal of Nuclear Materials, 2002, **307–311**: 1629–1636
30 WU Yi-Can, SONG Gang, CAO Rui-Fen et al. Chinese Physics C (HEP & NP), 2008, **32**(Suppl. II): 177–182
31 Bolch W E, Eckerman K F, Sgouros G et al. J Nucl. Med., 2009, **50**: 477–484. [PubMed: 19258258]
32 ICRP. 1979 Limits for Intakes of Radionuclides by Workers: Part 1 ICRP Publication 30 (Oxford: Pergamon), 1979
33 ICRP. ICRP Publication 107: Nuclear Decay Data for Dosimetric Calclations. Ann ICRP. 2008b, **38**: 1–26. [PubMed: 19154964]